


**Please cite the Published Version**

Li, Zhen, Meng, Zhaozeng, Soutis, Constantinos, Wang, Ping and Gibson, Andrew  (2022) Detection and analysis of metallic contaminants in dry foods using a microwave resonator sensor. Food Control, 133 (Part B). p. 108634. ISSN 0956-7135

**DOI:** <https://doi.org/10.1016/j.foodcont.2021.108634>

**Publisher:** Elsevier

**Version:** Accepted Version

**Downloaded from:** <https://e-space.mmu.ac.uk/629853/>

**Usage rights:**  [Creative Commons: Attribution-Noncommercial-No Derivative Works 4.0](https://creativecommons.org/licenses/by-nc-nd/4.0/)

**Additional Information:** This is an Accepted Manuscript of an article which appeared in Food Control, published by Elsevier

**Enquiries:**

If you have questions about this document, contact [openresearch@mmu.ac.uk](mailto:openresearch@mmu.ac.uk). Please include the URL of the record in e-space. If you believe that your, or a third party's rights have been compromised through this document please see our Take Down policy (available from <https://www.mmu.ac.uk/library/using-the-library/policies-and-guidelines>)

1 Detection and analysis of metallic contaminants in dry foods using a microwave resonator sensor

2 Zhen Li<sup>1\*</sup>, Zhaozong Meng<sup>2</sup>, Constantinos Soutis<sup>3</sup>, Ping Wang<sup>1</sup>, Andrew Gibson<sup>4</sup>

3  
4 <sup>1</sup>College of Automation Engineering, Nanjing University of Aeronautics and Astronautics,

5 Nanjing, 211106, China

6 <sup>2</sup>School of Mechanical Engineering, Hebei University of Technology, Tianjin, 300401, China

7 <sup>3</sup>Department of Materials, The University of Manchester, Manchester, M13 9PL, UK

8 <sup>4</sup>Faculty of Science and Engineering, Manchester Metropolitan University,

9 Manchester, M1 5GD, UK

10 \*Corresponding author: [zhenli@nuaa.edu.cn](mailto:zhenli@nuaa.edu.cn)

11 **Abstract**

12 Current systems for metal detection in dry food processing are limited by relatively large foreign  
13 objects and high-cost implementation. These issues are resolved here using a non-contact, cylindrical  
14 microwave cavity resonator sensor where food passes through the cavity and metallic objects are  
15 detected by a shift in the resonant frequency. Classic perturbation theory is applied to the basic set-  
16 up and numerical simulations are used to verify the design of the sensor. A cavity sensor was  
17 fabricated with a quartz tube symmetrically located for dry food flow and metal detection. Good  
18 performance is demonstrated for metal detection in a range of foods such as spaghetti, noodles, rice,  
19 wheat flour and soy milk powder. It is shown that the resonance frequency shift becomes larger  
20 when the foreign body gets closer to the cavity centre. The frequency variation is directly related to  
21 the volume of the object, and it is estimated that the minimum diameter of a detectable ball can be  
22 lower than 2 mm. For completeness it is also demonstrated that the set-up can be used to detect  
23 dielectric objects. A graphical user interface is developed for practical applications. This approach is  
24 low-cost, convenient, scalable and complementary to other metal contaminant detection approaches.

25  
26 **Keywords:** Dry foods; foreign objects; microwave technique; resonance frequency; cavity  
27 perturbation

## 29 1 Introduction

30 Foreign objects can be introduced into food products during harvesting, processing and final  
31 packing. Among all the contaminants, metallic objects (e.g., screws, bolts, nuts, small fragments  
32 from equipment in the production line or cleaning tools) cause the most concern for manufacturers if  
33 they are undetected and become embedded in final products, posing a severe threat to human health.  
34 A brand can be severely affected by such incidents. In addition, metal contamination may potentially  
35 damage the machinery, leading to unwanted downtime. Hence, from the economic point of view, it is  
36 of great importance to detect metal objects in food. Many non-invasive techniques have been  
37 developed. However, each has its advantages and limitations, and only one technique cannot serve  
38 all the needs of the industry. For example, the X-ray (Einarsdóttir et al., 2016; Morita, Ogawa, Thai,  
39 & Tanaka, 2003) and nuclear magnetic resonance (NMR) instruments are expensive and need high  
40 power usage. For the conventional liquid-coupled ultrasonics (Zhao, Basir, & Mittal, 2003), waves  
41 cannot propagate well in the air, and this can be overcome if the food is immersed in water. This  
42 special arrangement is not desirable for some food types, especially dry foods. Instead, air-coupled  
43 ultrasonics can be applied, while the point scanning feature impedes fast inspection. Terahertz  
44 inspection needs intricate instrumentation (Wang, Zhou, Huang, Xie, & Ying, 2019) and it has a low  
45 signal-to-noise ratio (Kim et al., 2012). Near-infrared (NIR) spectroscopy, thermal imaging and  
46 optical techniques cannot readily examine subsurface foreign bodies. Three types of widely used  
47 low-frequency electromagnetic detection systems are pulse technology, ferrous in foil detection, and  
48 the balanced three coil system (Craig, 2004). The pulse technology is limited to finding relatively  
49 large pieces of metals, like nails and cans. Ferrous in foil detectors are more suited to ferrous metal  
50 contamination. In a balanced three coil system, a transmitter and two receiver coils are used, and  
51 complicated signal processing is involved. Therefore, there is continued search for efficient  
52 identification of metallic objects.

53 In recent years, microwaves-based detection techniques have received increased attention. The  
54 microwave frequencies range from 300 MHz (wavelength of  $\sim 1$  m) to 300 GHz (wavelength of  $\sim 1$   
55 mm). In the analysis of the interaction with dielectrics, the complex permittivity (also called  
56 dielectric properties) is involved, and it can be characterised by  $\epsilon_0 \epsilon_r = \epsilon_0 (\epsilon_r' - j \epsilon_r'')$ .  $\epsilon_0$  is the electric  
57 permittivity of free space (i.e.,  $8.854 \times 10^{-12}$  F/m), and  $\epsilon_r$  is the relative permittivity.  $\epsilon_r'$  and  $\epsilon_r''$  are the  
58 real and imaginary parts of  $\epsilon_r$ , respectively.  $\epsilon_r'$  (commonly called dielectric constant) is related to the  
59 ability of energy storage.  $\epsilon_r''$  accounts for the energy dissipation. The microwave methods have  
60 several distinctive characteristics, such as low signal power consumption (few milliwatts), non-

61 contact inspection, ease of experimental setup, good repeatability and no-ionising radiation. They  
62 have been successfully applied for material characterisation (Brinker, Dvorsky, Al Qaseer, &  
63 Zoughi, 2020; Cuenca, Slocombe, & Porch, 2017; Li, Haigh, Soutis, & Gibson, 2019), damage  
64 evaluation (Li, Haigh, Soutis, & Gibson, 2018; Li, Wang, Haigh, Soutis, & Gibson, 2021) and food  
65 analysis (Li, Haigh, Soutis, Gibson, & Sloan, 2017; Li, Meng, Haigh, Wang, & Gibson, 2021; Li,  
66 Haigh, Wang, Soutis, & Gibson, 2021b, 2021a; Sosa-Morales, Valerio-Junco, López-Malo, &  
67 García, 2010). However, for contamination monitoring, little research can be found in the literature.  
68 Urbinati et al. (2020) developed a microwave system where six monopole antennas were arranged  
69 above packaged jars. Machine learning was incorporated to interpret the 6×6 matrix of scattering  
70 parameters. It was found that a metal sphere with a diameter of 10 mm was accurately detected by  
71 the multilayer perceptron classifier. In this approach, complicated signal post-processing was  
72 involved, impeding its wide application.

73 The primary objective of this study is to offer a novel approach for the detection of metals in food  
74 using microwave resonance. Dry foods are the food type of interest in the present work. The  
75 microwave energy is easily absorbed in moist samples and the resonance can be severely degraded.  
76 In comparison, in dry foods relating to a small  $\epsilon_r''$  value, lower energy is absorbed and consequently  
77 the signal penetration is deeper. It is noted that microwaves have very low penetration in metals,  
78 which behave more like reflectors and little electromagnetic energy is absorbed (Thostenson &  
79 Chou, 1999). By the insertion of a metallic object, a perturbation in the shape of a resonant cavity  
80 can be produced. Hence, here a low-cost cylindrical cavity resonator sensor is developed. The  
81 detection principle is described in detail, where the change of the resonance frequency is chosen as  
82 the primary indicator. Numerical simulation and experiments are carried out for verification. In the  
83 test, metallic objects in spaghetti are analysed first as an example, where the effects of the position,  
84 volume, quantity and shape of the object on the signal magnitude are thoroughly investigated.  
85 Finally, the detection performance for other dry foods including noodles, rice, wheat flour and soy  
86 milk powder is examined. The applicability of the sensor for dielectric contaminants is also studied.

## 87 **2 Materials and methods**

### 88 **2.1 Samples under test**

89 Five types of dry food samples bought from a local supermarket were measured, i.e., spaghetti,  
90 noodles, rice, wheat flour and soy milk powder. The diameter and length of the spaghetti strand were  
91 approximately 1.70 mm and 264 mm, respectively. Each noodle strand had a square cross section of  
92 approximately 1 mm×1 mm and a length of 184 mm. Metallic balls and wires, dielectric rods were

93 used as foreign bodies, material types and dimensions of which are listed in Table 1. Some reference  
 94 permittivity data of the samples are presented in Table 2. The sizes were measured with a digital  
 95 calliper (Pro's Kit Co. Ltd., Shanghai, China), which had an accuracy of 0.01 mm.

## 96 2.2 Microwave resonator sensor

97 The resonant cavity sensor was made of aluminium, which has a high electrical conductivity and is  
 98 reasonably priced. Its fabrication cost was around US\$ 75. As illustrated in Figure 1, the sensor  
 99 consists of a cylindrical wall and an endplate, which are mechanically connected by eight bolts and  
 100 nuts. The radius of the cavity ( $a$ ) is 47.5 mm, and the height ( $d$ ) is 40 mm. Two SubMiniature  
 101 version A (SMA) connectors are mounted on the endplate, and at the end of each connector a  
 102 coupling loop is made for the excitation of the resonant mode designated, i.e., TE<sub>011</sub> mode. For the  
 103 air-filled cavity designed, the resonance frequency can be computed by

$$104 \quad f_r = \frac{c}{2\pi} \sqrt{\left(\frac{p'_{01}}{a}\right)^2 + \left(\frac{\pi}{d}\right)^2} \quad (1)$$

105 where  $c$  is the speed of light in free space.  $p'_{01}=3.832$  is the first root of the derivative of  $J_0$ , which is  
 106 the Bessel function of first kind. Hence, by substituting the values of  $a$  and  $d$  into Equation (1), the  
 107 theoretical  $f_r$  value is approximately 5.3721 GHz.

108 The TE<sub>011</sub> mode has a degenerate mode (i.e., the TM<sub>111</sub> mode) that shares the same frequency but  
 109 exhibits different field distributions. To remove the mode interference, a hole with a diameter of 26  
 110 mm was drilled axially. The recess can be viewed as a short circular waveguide, and the cutoff  
 111 frequency of the dominant mode (approximately 6.76 GHz) is higher than the resonance frequency.  
 112 Thus, the electromagnetic energy can still be confined within the cavity.

## 113 2.3 Cavity perturbation caused by dielectrics and metals

114 When a dielectric sample like food is inserted into a resonant cavity, material perturbation is  
 115 introduced. The fractional change in the resonant frequency can be estimated by (Collin, 2000)

$$116 \quad \frac{\omega_2 - \omega_1}{\omega_1} \approx \frac{-\int_{V_c} (\Delta\varepsilon |\bar{E}_1|^2 + \Delta\mu |\bar{H}_1|^2) dv}{\int_{V_c} (\varepsilon |\bar{E}_1|^2 + \mu |\bar{H}_1|^2) dv} \quad (2a)$$

$$117 \quad \omega_1 = 2\pi f_1 + \frac{j\pi f_1}{Q_1} \quad (2b)$$

$$118 \quad \omega_2 = 2\pi f_2 + \frac{j\pi f_2}{Q_2} \quad (2c)$$

119 where  $\omega_1, f_1$  and  $Q_1$  are the complex angular frequency, resonance frequency and quality factor  
 120 before the perturbation, respectively.  $\omega_2, f_2$  and  $Q_2$  are the complex angular frequency, resonance  
 121 frequency and quality factor after the perturbation, respectively.  $\varepsilon$  and  $\mu$  are the electric permittivity  
 122 and magnetic permeability of the medium in the unperturbed cavity, respectively. In the present case,  
 123  $\varepsilon$  and  $\mu$  are equal to  $\varepsilon_0$  and magnetic permeability of free space  $\mu_0=4\pi\times 10^{-7}$  H/m, respectively.  $\Delta\varepsilon$  and  
 124  $\Delta\mu$  are the permittivity and permeability changes introduced by the sample, respectively. Thus,  $\Delta\varepsilon$   
 125 can be expressed as  $\varepsilon_0[(\varepsilon'_r-1)-j\varepsilon''_r]$ . The dielectrics are generally non-magnetic, so  $\Delta\mu$  is equivalent to  
 126 zero.  $\bar{E}_1$  and  $\bar{H}_1$  are the original electric and magnetic fields, respectively.  $V_c$  is the volume of the  
 127 cavity. For the original cavity, at resonance the electric energy stored in the cavity volume is equal to  
 128 the magnetic energy stored, i.e.,

$$129 \int_{V_c} \varepsilon |\bar{E}_1|^2 dv \approx \int_{V_c} \mu |\bar{H}_1|^2 dv \quad (3)$$

130 Hence, the resonance frequency  $\Delta f_r=f_2-f_1$  can be given by

$$131 \Delta f_r \approx -\frac{(\varepsilon'_r-1)f_1 \int_{V_d} |\bar{E}_1|^2 dv}{2 \int_{V_c} |\bar{E}_1|^2 dv} \quad (4)$$

132 where  $V_d$  is the volume of the dielectric object. It is indicated that a lower resonance frequency can  
 133 be produced by the food, and the frequency change is larger for a higher dielectric constant.  
 134 When the food contains a metallic object, the volume of the cavity is slightly reduced, causing  
 135 additional shape perturbation. The resultant resonance frequency change can be approximated by  
 136 (Pozar, 2012)

$$137 \frac{\Delta f_r}{f_1} \approx \frac{\int_{V_m} (\mu |\bar{H}_1|^2 - \varepsilon |\bar{E}_1|^2) dv}{\int_{V_c} (\mu |\bar{H}_1|^2 + \varepsilon |\bar{E}_1|^2) dv} \quad (5)$$

138 where  $V_m$  is the volume of the metallic object. Resonance frequencies  $f_1$  and  $f_2$  correspond to food  
 139 without and with a metallic object inside, respectively. For the TE<sub>011</sub> mode, as the electric field  
 140 intensity around the axis is relatively low, the magnetic field is more affected. Therefore, the  
 141 resonance frequency would be increased when a metallic object appears. Considering the extreme  
 142 case where the contribution by  $\bar{E}_1$  is ignored, the expression for  $\Delta f_r$  can be simplified as

$$143 \Delta f_r \approx \frac{V_m f_1}{2} \frac{|\bar{H}_{1,avg}|^2}{\int_{V_c} |\bar{H}_1|^2 dv} \quad (6)$$

144 where  $|\bar{H}_{1,\text{avg}}|$  is the average magnetic field intensity in the metallic object region.  $\Delta f_r$  is directly  
 145 proportional to  $V_m$ , suggesting that the detection is more sensitive to a larger object.  
 146 Using the shape perturbation theory, the resonant mode can be checked with a metallic wire  
 147 positioned along the cavity axis. The wire has a small radius  $r$  and a length longer than the cavity  
 148 height.  $r$  can be estimated from the resonant frequency shift by substituting the expressions of the  
 149 electric and magnetic fields of the desired resonant mode into Equation (5). For the TE<sub>011</sub> mode,  $r$   
 150 can be given by

$$151 \quad r \approx a \sqrt{2\zeta \frac{\Delta f_r}{f_1}} \quad (7)$$

152 where the coefficient  $\zeta$  is expressed as

$$153 \quad \zeta = \left[ 1 + \left( \frac{\pi a}{dp'_{01}} \right)^2 \right] J_0^2(p'_{01}) \quad (8)$$

154 If the  $r$  value calculated is close to the real value, the resonant mode can be confirmed.

## 155 2.4 Experimental setup

156 The setup for the food examination using the microwave resonator sensor is shown in Figure 2. The  
 157 sensor was connected to a portable N9951A Fieldfox microwave analyser (Keysight Technologies,  
 158 Penang, Malaysia) by two coaxial cables. A LAN cable was used to link the analyser to a personal  
 159 computer (PC). As a two-port measurement, the transmission coefficient ( $S_{21}$ ) data were extracted. In  
 160 the test, the default signal power (i.e., 0.032 mW) was adopted.

161 A frequency span of 20 MHz with 401 points was used, so that the frequency resolution was 0.05  
 162 MHz. The intermediate frequency bandwidth (IFBW) was set to 100 Hz to reduce the noise floor and  
 163 accurately measure the non-resonance region. The analyser setting produced a long sweep time of  
 164 around 10.3 s. To shorten the time for rapid online monitoring, the number of points can be set lower  
 165 and/or IFBW value can be set higher without significantly decreasing the detection accuracy, as only  
 166 the resonance frequency value is needed and the peak signal is orders of magnitude larger than the  
 167 non-resonance region. For a frequency range of 5.324-5.334 GHz with 101 points (the corresponding  
 168 frequency resolution was 0.10 MHz, which was still enough for discrimination) and an IFBW value  
 169 of 10 kHz, the sweep time was approximately 66 ms.

170 For easy positioning of the sample, a 160 mm long quartz tube with an inner diameter of 12 mm and  
 171 an outer diameter of 14 mm was used. The food sample was filled into the tube and inserted into the  
 172 resonant cavity through two cuboid-shaped tube holders. Each tube holder had a central hole with a  
 173 diameter of 14 mm and was attached to the top and bottom surfaces of the cavity.

174

## 175 **3 Results and discussion**

### 176 **3.1 Electromagnetic simulation**

177 CST<sup>®</sup> software is employed for the feasibility study. The cavity model built is given in Figure 3 (a),  
178 and the electric and magnetic field distributions are presented in Figure 3 (b-d), where the patterns  
179 produced match those of the ideal TE<sub>011</sub> mode, validating the cavity design. The magnetic field  
180 intensity is the highest at the cavity centre, where the presence of a metallic object can cause a  
181 relatively large perturbation. It is also shown that the magnetic field intensity is high around the axis,  
182 but the electric field intensity is relatively low. Hence, a perturbation can be more easily generated  
183 by a metal than a dielectric.

184 Three representative cases are considered, i.e., an empty cavity, insertion of a quartz tube and a  
185 copper sphere. The relative permittivity data of fused quartz,  $3.75-j1.5\times 10^{-3}$ , is from the built-in  
186 material library. The resonance frequency of the empty cavity simulated is 5.3634 GHz, which is in  
187 good agreement with the theoretical value (an error of 0.2%). As seen in Figure 4 (a), with the  
188 introduction of a quartz tube, the resonance frequency is shifted to 5.3432 GHz due to material  
189 perturbation. A copper sphere is further created at the cavity centre, and the resonance peak shifts  
190 upwards with increasing sphere diameter ( $D=1, 2, 3, 4, 5$  mm). The perturbation of the magnetic  
191 field around the sphere is shown in Figure 4 (b) and (c), where only the field lines close to the sphere  
192 surface are distorted and the small perturbation condition is satisfied. The effect of the diameter on  
193 the resonance frequency shift is plotted in Figure 4 (d), where a linear correlation with a high  
194 coefficient of determination  $R^2=0.999$  is given and the intercept of the fitted equation obtained is  
195 small compared with the dynamic range of the frequency shift. The findings agree well with the  
196 theoretical analysis (i.e., Equation (6)).

### 197 **3.2 Experimental results**

#### 198 **3.2.1 Examination of the resonant mode**

199 The resonant mode was checked with the LWb wire, and another similar tube holder with a central  
200 hole of the same diameter as the wire was made. For the empty cavity, one resonance peak was  
201 observed over 5.34-5.38 GHz, and the resonance frequency measured was 5.35362 GHz (only 0.4%  
202 lower than the theoretical value). When the wire was inserted, the peak shifted to 5.36264 GHz.  
203 Using the cavity dimensions and resonance frequencies measured, the radius computed was 1.55 mm,  
204 and the resultant error was well within 5%, demonstrating that the resonance frequency measured  
205 corresponded to the TE<sub>011</sub> mode and the degenerate mode was successfully suppressed.



### 206 3.2.2 *Characterisation of a metallic ball in spaghetti*

207 The quartz tube was partially filled with 17 spaghetti strands to mimic the real scenario where the  
208 food shall freely flow in the production line. The height of the spaghetti was around 6 mm (i.e., the  
209 radius of the tube). First, a BD5 ball was placed below the spaghetti at a position just outside the  
210 cavity, i.e., P0 as illustrated in Figure 5 (a). After the measurement at this position, the tube together  
211 with the spaghetti and ball was moved to the other ten positions (denoted by P1-P10). The distance  
212 between the adjacent positions was 5mm. Starting from P3, the ball entered the cavity. At P7 the ball  
213 was located closest to the cavity centre. During the movement, the length of the spaghetti part in the  
214 cavity was always equal to the cavity height.

215 The resonant responses for all the positions are given in Figure 5 (b). The frequency decreased when  
216 the spaghetti was placed into the empty cavity. The frequency changes with respect to P0 are  
217 computed and presented in Figure 5 (c). Three consecutive measurements were done for each case,  
218 while the resonance frequency extracted remained the same due to the low IFBW value used,  
219 demonstrating good repeatability of the sensor. Therefore, error bars are not plotted in the figure. The  
220 highest frequency shift  $\Delta f_r$  was seen at P7 as would be expected. For comparison, the spaghetti  
221 without the presence of the ball were measured at the eleven positions as well, and the maximum  
222 difference between the frequencies was 0.15 MHz, indicating a relatively low noise.

223 The P0 case is different from the spaghetti-only case, as there is a resonance frequency difference of  
224 1.75 MHz. At P0 the ball did not affect the magnetic field distribution in the cavity, but the spaghetti  
225 were lifted upwards due to the relatively high stiffness of the spaghetti. As indicated by the  
226 simulation, when the centre of the material is closer to the cavity axis, the electric field intensity  
227 inside becomes smaller. Therefore, according to the material perturbation theory, the frequency  
228 becomes higher than that of the spaghetti-only case. Hence, it is suggested that the sensor can detect  
229 the presence of a metal when it is close to but still not in the cavity.

230 As shown in Figure 5 (c), smaller balls (i.e., BD2, BD3 and BD4) are also detected. A smaller object  
231 produces a lower  $\Delta f_r$ , which agrees well with Equation (6). A similar linear relationship is found  
232 between the maximum  $\Delta f_r$  at P7 and the cube of the diameter  $D$ , i.e.,  $\Delta f_r = 0.0421D^3 - 0.1223$  with  
233  $R^2 = 0.9909$ . Considering the signal noise, the minimum diameter of a ball that can be detected in the  
234 spaghetti is around 1.86 mm.

### 235 3.2.3 *Effect of the ball quantity on the signal responses*

236 Taking the BD3 ball as an example, the effect of the ball quantity was studied. The balls were in  
237 contact and aligned in parallel to the cavity axis. Initially, the centre of the balls was at P0. The  
238 differences between the resonance frequencies at P0 and P7 are listed in Table 3, where the

239 placement of more balls leads to a greater frequency shift. The responses for a large number of balls  
240 were evaluated using the LWa and LWb wires, where the latter had the same diameter as the BD3  
241 ball. The frequency shift caused was higher than any of the ball cases as expected. In comparison, the  
242 LWa wire had a smaller diameter, and a lower  $\Delta f_r$  was obtained.

#### 243 **3.2.4 Detection of a short wire in spaghetti**

244 Same as the balls, short wires were measured at P0 and P7. The corresponding resonance frequency  
245 differences are presented in Table 4, where lower responses are seen for smaller dimensions. In the  
246 test, the wire was parallel to the magnetic field, and the cross-sectional area was smaller than the  
247 diameter of a ball of the same volume (e.g., SWb2 and BD4), thereby inducing weaker perturbation.  
248 Thus, it is indicated that ball-shaped objects can be more easily identified than stick-shaped objects.

### 249 **3.3 Discussion**

#### 250 **3.3.1 Detection of a metallic object in other dry foods**

251 Same as the setup in the spaghetti cases, the sensor performance for the other dry food samples was  
252 examined. For each sample, the two cases with food only and with a BD3 ball at P7 were considered.  
253 The resonant responses obtained are presented in Figure 6, where the  $\Delta f_r$  values for noodles, rice,  
254 wheat flour and soy milk powder are 2.75 MHz, 3.68 MHz, 2.93 MHz and 2.03 MHz, respectively.  
255 Thus, the ball can be readily detected in these foods as well. For the noodles, the effect of the ball  
256 size was also studied at P0 and P7, and the  $\Delta f_r$  values for BD2, BD3, BD4 and BD5 were 0.20 MHz,  
257 0.95 MHz, 2.75 MHz and 5.85 MHz, respectively. For the same ball, the value of  $\Delta f_r$  is slightly  
258 higher than that in the spaghetti case, indicating better detection sensitivity. The trend of the  
259 frequency shift with respect to the ball size (the relationship between  $\Delta f_r$  and  $D^3$  is  $\Delta f_r=0.0487D^3-$   
260  $0.2922$  with  $R^2=0.9987$ ) is consistent with that for spaghetti.

#### 261 **3.3.2 Examination of a dielectric object in spaghetti**

262 The sensitivity to a dielectric object was investigated using short Plexiglas rods. The  $\Delta f_r$  values  
263 computed at P1-P10 for four rods with varied lengths are presented in Figure 7, where the frequency  
264 decreases as the rod is closer to the cavity centre. This trend of the frequency variation is opposite to  
265 that for a metallic object, facilitating the differentiation of metallic and dielectric objects. The  
266 primary reason is due to the fact that here material perturbation is involved. Compared with the  
267 results of the metallic balls given in Figure 5 (c), the signal magnitudes for the rods are five times  
268 lower, though the volumes are comparable. Therefore, it is suggested that the Plexiglas material is  
269 less detectable.

270 **3.3.3 Development of foreign object detection software**

271 As shown in Figure 8, MATLAB GUI-based software is programmed for easier identification of a  
272 foreign body. First, six parameter values are input for analyser setting and analyser-computer  
273 communication, i.e., IEEE GPIB address, start frequency, stop frequency, number of points, IFBW  
274 value and signal power.  $S_{21}$  data from a reference case (e.g., a foreign body-free case) are taken.  
275 Continuous scanning is then performed until the current resonance frequency shift is over the  
276 detection threshold defined. A warning message box pops up when a foreign object is found, and the  
277 specific object type (metal or dielectric) is also provided.

278 **4 Concluding remarks**

279 A new microwave resonant system has been introduced for the detection of metals in dry foods. The  
280 low-cost sensor requires very low signal power and is sensitive to both ferrous and non-ferrous  
281 containments. The presence of a metallic object perturbs the magnetic field in the  $TE_{011}$  mode  
282 resonant cavity and causes an increase in the resonance frequency. In the evaluation of metallic balls  
283 in spaghetti, it has been revealed that the frequency shift is proportional to the volume of the ball,  
284 which is in good agreement with the theoretical analysis and numerical simulation. The minimum  
285 diameter of a detectable ball can be lower than 2 mm. For the same volume, an object with a larger  
286 cross-sectional area can be identified more easily due to the stronger perturbation. Good detection  
287 performance has also been shown for other types of dry foods. The sensor can also be applied for the  
288 detection of dielectric containments. For the low electric field intensity around the axis and small  
289 difference of the permittivity between the dry food and the foreign object, the detection signal is  
290 relatively low compared with a metal of the same volume. A GUI-based programme has been  
291 developed for convenient implementation. The comparison between the proposed sensor and the  
292 existing research for foreign body detection in dry foods is presented in Table 5.

293 In future work, the speed of the moving food on the effectiveness of the sensor system is to be tested.  
294 Methods like gold plating on the inner surface of the cavity, use of more frequency points and  
295 minimisation of the recess size will be adopted to improve the sensor performance. In addition,  
296 bespoke low-cost sensor electronics will be developed for industrial use. For a real production line,  
297 the cavity can be scaled up to ensure high throughput, and the technique can be combined with other  
298 non-invasive sensors for enhanced performance.

299  
300  
301  
302

303 **Acknowledgements**

304 This work was financially supported by the Natural Science Foundation of Jiangsu Province (Grant  
305 No. BK20200427), the Shuangchuang Project of Jiangsu Province (Grant No. KFR20020), the  
306 Fundamental Research Funds for the Central Universities (Grant No. NS2020019) and the National  
307 Natural Science Foundation of China (Grant No. 52105552). The first author gratefully  
308 acknowledges Dr.Changcheng Wu and Dr. Fei Fei for assistance in the experiments.

309

310 **References**

- 311 A. Prasad, & P. N. Singh. (2007). A New Approach to Predicting the Complex Permittivity of Rice.  
312 *Transactions of the ASABE*, 50(2), 573–582. <https://doi.org/10.13031/2013.22645>
- 313 Brinker, K., Dvorsky, M., Al Qaseer, M. T., & Zoughi, R. (2020). Review of advances in microwave  
314 and millimetre-wave NDT&E: principles and applications. *Philosophical Transactions of*  
315 *the Royal Society A: Mathematical, Physical and Engineering Sciences*, 378(2182), 20190585.  
316 <https://doi.org/10.1098/rsta.2019.0585>
- 317 Collin, R. E. (2000). *Foundations for Microwave Engineering* (2nd ed.). Wiley-IEEE Press.
- 318 Craig, J. P. (2004). Metal detection. In M. Edwards (Ed.), *Detecting Foreign Bodies in Food* (p.  
319 306). Cambridge, England: CRC Press.
- 320 Cuenca, J. A., Slocombe, D. R., & Porch, A. (2017). Temperature Correction for Cylindrical Cavity  
321 Perturbation Measurements. *IEEE Transactions on Microwave Theory and Techniques*, 65(6),  
322 2153–2161. <https://doi.org/10.1109/TMTT.2017.2652462>
- 323 Einarsdóttir, H., Emerson, M. J., Clemmensen, L. H., Scherer, K., Willer, K., Bech, M., ... Pfeiffer,  
324 F. (2016). Novelty detection of foreign objects in food using multi-modal X-ray imaging. *Food*  
325 *Control*, 67, 39–47. <https://doi.org/10.1016/j.foodcont.2016.02.023>
- 326 Ginesu, G., Giusto, D. D., Margner, V., & Meinschmidt, P. (2004). Detection of foreign bodies in  
327 food by thermal image processing. *IEEE Transactions on Industrial Electronics*, 51(2), 480–  
328 490. <https://doi.org/10.1109/TIE.2004.825286>
- 329 Hippel, A. R. Von. (1995). *Dielectric materials and applications* (2nd ed.). New York: Artech  
330 House. Retrieved from <http://cds.cern.ch/record/270934>
- 331 Kim, G.-J., Kim, J.-I., Jeon, S.-G., Kim, J., Park, K.-K., & Oh, C.-H. (2012). Enhanced Continuous-  
332 Wave Terahertz Imaging with a Horn Antenna for Food Inspection. *Journal of Infrared,*  
333 *Millimeter, and Terahertz Waves*, 33(6), 657–664. <https://doi.org/10.1007/s10762-012-9902-1>
- 334 Kwon, J.-S., Lee, J.-M., & Kim, W.-Y. (2008). Real-time detection of foreign objects using X-ray  
335 imaging for dry food manufacturing line. In *2008 IEEE International Symposium on Consumer*

336 *Electronics* (pp. 1–4). IEEE. <https://doi.org/10.1109/ISCE.2008.4559552>

337 Li, Z., Haigh, A., Soutis, C., & Gibson, A. (2018). Principles and Applications of Microwave Testing  
338 for Woven and Non-Woven Carbon Fibre-Reinforced Polymer Composites: a Topical Review.  
339 *Applied Composite Materials*, 25(4), 965–982. <https://doi.org/10.1007/s10443-018-9733-x>

340 Li, Z., Haigh, A., Soutis, C., & Gibson, A. (2019). X-band microwave characterisation and analysis  
341 of carbon fibre-reinforced polymer composites. *Composite Structures*, 208, 224–232.  
342 <https://doi.org/10.1016/j.compstruct.2018.09.099>

343 Li, Z., Haigh, A., Soutis, C., Gibson, A., & Sloan, R. (2017). Evaluation of water content in honey  
344 using microwave transmission line technique. *Journal of Food Engineering*, 215, 113–125.  
345 <https://doi.org/10.1016/j.jfoodeng.2017.07.009>

346 Li, Z., Haigh, A., Wang, P., Soutis, C., & Gibson, A. (2021a). Characterisation and analysis of  
347 alcohol in baijiu with a microwave cavity resonator. *LWT*, 141, 110849.  
348 <https://doi.org/10.1016/j.lwt.2021.110849>

349 Li, Z., Haigh, A., Wang, P., Soutis, C., & Gibson, A. (2021b). Dielectric spectroscopy of Baijiu over  
350 2–20 GHz using an open-ended coaxial probe. *Journal of Food Science*, 86(6), 2513–2524.  
351 <https://doi.org/10.1111/1750-3841.15738>

352 Li, Z., Meng, Z., Haigh, A., Wang, P., & Gibson, A. (2021). Characterisation of water in honey using  
353 a microwave cylindrical cavity resonator sensor. *Journal of Food Engineering*, 292, 110373.  
354 <https://doi.org/10.1016/j.jfoodeng.2020.110373>

355 Li, Z., Wang, P., Haigh, A., Soutis, C., & Gibson, A. (2021). Review of microwave techniques used  
356 in the manufacture and fault detection of aircraft composites. *The Aeronautical Journal*,  
357 125(1283), 151–179. <https://doi.org/10.1017/aer.2020.91>

358 Mason, P. R., Hasted, J. B., & Moore, L. (1974). The use of statistical theory in fitting equations to  
359 dielectric dispersion data. *Advances in Molecular Relaxation Processes*, 6(3), 217–232.  
360 [https://doi.org/10.1016/0001-8716\(74\)80003-9](https://doi.org/10.1016/0001-8716(74)80003-9)

361 Morita, K., Ogawa, Y., Thai, C. N., & Tanaka, F. (2003). Soft X-Ray Image Analysis to Detect  
362 Foreign Materials in Foods. *Food Science and Technology Research*, 9(2), 137–141.  
363 <https://doi.org/10.3136/fstr.9.137>

364 Nelson, S. O. (1984). Density Dependence of the Dielectric Properties of Wheat and Whole-Wheat  
365 Flour. *Journal of Microwave Power*, 19(1), 55–64.  
366 <https://doi.org/10.1080/16070658.1984.11689350>

367 Ok, G., Kim, H. J., Chun, H. S., & Choi, S.-W. (2014). Foreign-body detection in dry food using  
368 continuous sub-terahertz wave imaging. *Food Control*, 42, 284–289.

369 <https://doi.org/10.1016/j.foodcont.2014.02.021>

370 Pallav, P., Hutchins, D. A., & Gan, T. . (2009). Air-coupled ultrasonic evaluation of food materials.  
371 *Ultrasonics*, 49(2), 244–253. <https://doi.org/10.1016/j.ultras.2008.09.002>

372 Pozar, D. M. (2012). *Microwave Engineering*. John Wiley & Sons, Inc. (Fourth edi). New York: John  
373 Wiley & Sons. <https://doi.org/10.1007/s13398-014-0173-7.2>

374 Sosa-Morales, M. E., Valerio-Junco, L., López-Malo, A., & García, H. S. (2010). Dielectric  
375 properties of foods: Reported data in the 21st Century and their potential applications. *LWT -*  
376 *Food Science and Technology*, 43(8), 1169–1179. <https://doi.org/10.1016/j.lwt.2010.03.017>

377 Stuart O. Nelson, & Tian-su You. (1989). Microwave Dielectric Properties of Corn and Wheat  
378 Kernels and Soybeans. *Transactions of the ASAE*, 32(1), 0242–0249.  
379 <https://doi.org/10.13031/2013.30990>

380 Thostenson, E. T., & Chou, T. W. (1999). Microwave processing: fundamentals and applications.  
381 *Composites Part A: Applied Science and Manufacturing*, 30(9), 1055–1071.  
382 [https://doi.org/10.1016/S1359-835X\(99\)00020-2](https://doi.org/10.1016/S1359-835X(99)00020-2)

383 Urbinati, L., Ricci, M., Turvani, G., Vasquez, J. A. T., Vipiana, F., & Casu, M. R. (2020). A  
384 Machine-Learning Based Microwave Sensing Approach to Food Contaminant Detection. In  
385 *2020 IEEE International Symposium on Circuits and Systems (ISCAS)* (pp. 1–5). IEEE.  
386 <https://doi.org/10.1109/ISCAS45731.2020.9181293>

387 Wang, C., Zhou, R., Huang, Y., Xie, L., & Ying, Y. (2019). Terahertz spectroscopic imaging with  
388 discriminant analysis for detecting foreign materials among sausages. *Food Control*, 97, 100–  
389 104. <https://doi.org/10.1016/j.foodcont.2018.10.024>

390 Yin, J., Hameed, S., Xie, L., & Ying, Y. (2021). Non-destructive detection of foreign contaminants  
391 in toast bread with near infrared spectroscopy and computer vision techniques. *Journal of Food*  
392 *Measurement and Characterization*, 15(1), 189–198. [https://doi.org/10.1007/s11694-020-](https://doi.org/10.1007/s11694-020-00627-6)  
393 [00627-6](https://doi.org/10.1007/s11694-020-00627-6)

394 Zhao, B., Basir, O. A., & Mittal, G. S. (2003). Detection of metal, glass and plastic pieces in bottled  
395 beverages using ultrasound. *Food Research International*, 36(5), 513–521.  
396 [https://doi.org/10.1016/S0963-9969\(02\)00201-6](https://doi.org/10.1016/S0963-9969(02)00201-6)

397

398 **Tables**

399

400

Table 1 Details of the foreign objects used in this study

	Ball				Long wire				Short wire				Short rods			
Material	Q235 steel				Copper				Copper				Plexiglass			
Diameter (mm)	2.00	3.00	3.98	5.02	1.70	2.97	2.66	2.66	2.18	2.18	1.70	1.70	3.12			
Length (mm)	-	-	-	-	201.00	201.00	20.03	10.16	20.20	10.04	20.10	10.16	4.06	6.20	7.90	20.25
Code	BD2	BD3	BD4	BD5	LWa	LWb	SWa1	SWa2	SWb1	SWb2	SWc1	SWc2	PRa	PRb	PRc	PRd

401

402 Table 2 Reference permittivity data of the food samples and dielectric rod under investigation

Material	Rice	Wheat flour	Ground soybean	Plexiglas	Water
Reference	(A. Prasad & P. N. Singh, 2007)	(Nelson, 1984)	(Stuart O. Nelson & Tian-su You, 1989)	(Hippel, 1995)	(Mason, Hasted, & Moore, 1974)
$\epsilon_r$	2.32-j0.34 (2.45 GHz)	3.35-j0.34 (11.67 GHz)	4.02-j0.22 (11.5 GHz)	2.60-j0.01 (3 GHz) 2.59-j0.02 (10 GHz)	73.40-j18.16 (5 GHz)
Temperature (°C)	24	22	24	27	25
Moisture content (%)	11	8.5	7.5	N/A	N/A

403

404 Table 3 Effect of the object quantity on the resonance frequency difference between P0 and P7

	Number of the BD3 balls					LWa	LWb
	2	3	4	5	6		
$f_r$ at P0 (GHz)	5.32395	5.32395	5.32395	5.32390	5.32390	5.32445	5.32460
$f_r$ at P7 (GHz)	5.32685	5.32820	5.32915	5.32995	5.33045	5.32800	5.33220
$\Delta f_r$ (MHz)	2.90	4.25	5.20	6.05	6.55	3.55	7.60

405

406 Table 4 Resonance frequency shifts caused by the insertion of short copper wires in spaghetti

	SWa1	SWa2	SWb1	SWb2	SWc1	SWc2
Volume (mm <sup>3</sup> )	111.31	56.46	75.40	37.47	45.62	23.06
$f_r$ at P0 (GHz)	5.32645	5.32645	5.32630	5.32560	5.32560	5.32545
$f_r$ at P7 (GHz)	5.33040	5.32810	5.32880	5.32670	5.32675	5.32620
$\Delta f_r$ (MHz)	3.95	1.65	2.50	1.10	1.15	0.75

407

408

409

410

411

412

Table 5 Comparison between the proposed methodology and the existing detection methods

Non-invasive method	Food products	Foreign bodies	Advantages	Limitations
X-ray (Kwon, Lee, & Kim, 2008)	Instant ramen, macaroni and spaghetti	Balls made of stainless steel, Teflon, aluminium, rubber, glass and ceramic	<ul style="list-style-type: none"> <li>• High image resolution</li> <li>• Good penetration</li> </ul>	<ul style="list-style-type: none"> <li>• High cost</li> <li>• High power usage</li> <li>• Ionising radiation</li> </ul>
Air-coupled ultrasonics (Pallav, Hutchins, & Gan, 2009)	Chocolate	Hazelnut, mint	<ul style="list-style-type: none"> <li>• Non-contact inspection</li> <li>• Reasonable penetration</li> </ul>	<ul style="list-style-type: none"> <li>• Raster scanning required</li> <li>• Low signal-to-noise ratio</li> </ul>
Terahertz (Ok, Kim, Chun, & Choi, 2014)	Milk powder	Steel nuts and washers, square and circular polymer samples, insects	<ul style="list-style-type: none"> <li>• Non-contact inspection</li> </ul>	<ul style="list-style-type: none"> <li>• Intricate experimental setup</li> <li>• Low signal-to-noise ratio</li> <li>• Raster scanning required</li> </ul>
Near-infrared spectroscopy (Yin, Hameed, Xie, & Ying, 2021)	Toast bread	metal, plastic and hair	<ul style="list-style-type: none"> <li>• Full-field imaging</li> <li>• Reasonable image resolution</li> </ul>	<ul style="list-style-type: none"> <li>• Image processing required for better interpretation</li> <li>• Poor penetration</li> </ul>
Thermal imaging (Ginesu, Giusto, Margner, & Meinschmidt, 2004)	Raisins, almonds and nuts	Wooden sticks, stone, metal chips and cardboard pieces	<ul style="list-style-type: none"> <li>• Full-field imaging</li> </ul>	<ul style="list-style-type: none"> <li>• Relatively high power usage</li> <li>• Poor penetration</li> </ul>
Present work	Spaghetti, noodles, rice, wheat flour and soy milk powder	Metallic balls and wires, dielectric rods	<ul style="list-style-type: none"> <li>• Low power consumption</li> <li>• Easy signal interpretation</li> <li>• Low cost</li> <li>• Volumetric sensing</li> </ul>	<ul style="list-style-type: none"> <li>• Limited penetration for high-moisture materials</li> </ul>

413

414



415 **Figure captions**

416

417 Figure 1 Cross section of the microwave resonator sensor developed for food examination (not to  
418 scale)

419 Figure 2 Schematic diagram of the experimental setup for the detection of metallic contamination in  
420 dry foods using microwave resonance

421 Figure 3 Numerical simulation of the electric and magnetic fields in the microwave sensor at  
422 resonance: (a) cross-sectional view of the empty cavity model; (b) electric fields in the transverse  
423 plane; (c) electric fields in the  $y$ - $z$  plane (pointing out of the paper on the left-hand side and pointing  
424 to the paper on the right-hand side); (d) magnetic fields in the  $y$ - $z$  plane

425 Figure 4 Effect of a metallic sphere on the microwave resonance studied by simulation: (a) signal  
426 responses for the cavity with and without a sphere; (b) magnetic field distribution in the presence of  
427 the sphere; (c) close-up view of the magnetic field around the sphere; (d) variation of the resonance  
428 frequency shift with respect to the diameter ( $D$ ) of the sphere

429 Figure 5 Evaluation of a metallic ball in spaghetti using the microwave resonator sensor: (a)  
430 schematic diagram of the eleven positions along the axis for the study of the position effect; (b)  
431 resonant responses for the BD5 ball; (c) resonance frequency shift due to the movement of the ball  
432 from the original position into the cavity

433 Figure 6 Resonant responses for other dry foods with and without a metallic ball placed at P7

434 Figure 7 Resonance frequency shifts caused by dielectric rods at varied positions in the cavity

435 Figure 8 Self-developed GUI-based software for easy online detection of a foreign object in dry food  
436 (here a BD3 ball is placed in spaghetti)